Probing Surface-Adsorbate Interactions through Active Particle Dynamics

Benjamin Greydanus,[1] Mohammad Saleheen,[2] Haichao Wu,[1] Andreas Heyden,[2] J. Will Medlin,[1] and Daniel K. Schwartz[1*]

[1] Department of Chemical and Biological Engineering, University of Colorado, Boulder, 596 UCB, Boulder, Colorado 80309, United States

[2] Department of Chemical Engineering, University of South Carolina, 301 Main Street, Columbia, South Carolina 29208, United States

[*] Corresponding author

E-mail: daniel.schwartz@colorado.edu

Phone: (303) 735-0240

Abstract

Adsorbate molecules present in a reaction mixture may bind to and block catalytic sites. Measurement of the surface coverage of these molecules via adsorption isotherms is critical for modeling and design of catalytic reactions on surfaces. However, it is challenging to measure isotherms in solution in a way that is directly relevant to catalytic activity under reaction conditions, particularly since adsorbates may bind with an enormous range of surface affinity parameters. Here we used the motion of self-propelled catalytic Janus particles, which employ the decomposition of hydrogen peroxide fuel as a propulsion mechanism, to determine the effective surface coverage of thioglycerol, furfural, and ethanol on a platinum surface as a function of concentration in aqueous solution by measuring the decrease in active motion due to the blocking of active sites. For strongly adsorbing thioglycerol, this effective coverage was compared and contrasted to the total adsorbed amount measured using inductively-coupled plasma analysis. Demonstrating the broad applicability of this approach, the surface affinity of the three adsorbates spanned more than four orders of magnitude. For each species, the adsorbate-mediated attenuation of active motion occurred over a wide concentration range and was well-described by a Langmuir isotherm. The strongly interacting thioglycerol had the highest affinity towards the surface (K_a = 15.5 ± 4.3 mM^{-1}) and fully deactivated the active particle motion at surface saturation. Furfural had an intermediate affinity (K_a = 0.42 ± 0.07 mM^{-1}) but did not fully block H_2O_2 access to the surface at apparent saturation, consistent with a maximum fractional surface coverage of θ_{max} = 0.67. Ethanol exhibited even lower affinity (K_a = 0.0025 ± 2x10^{-4} mM^{-1}) and its coverage saturated at only θ_{max} = 0.38. Analysis of isotherms at elevated temperatures enabled direct extraction of the enthalpies of adsorption. The degree of surface coverage at adsorbate saturation appeared to correlate with the relative energies of adsorption for the different adsorbate species and was consistent with adsorbate saturation of one of multiple active site populations towards H_2O_2 decomposition. Moreover, computational investigations into solvent effects on furfural adsorption showed good quantitative agreement with the experimental results. This work leverages unique properties of active particles to

explore fundamental catalysis questions and demonstrates a novel paradigm for significant and experimentally accessible multidisciplinary research.

Keywords: Active particles, catalysis, adsorption, surface coverage

1. Introduction

Adsorption of solute molecules at the liquid−solid interface is of central importance in liquid-phase heterogeneous catalysis. Reactant adsorption from solution onto the catalytic surface is typically required to initiate the reaction. Moreover, other solute species (or in some cases the solvent) can adsorb on the surface and compete with the reactant for catalytic active sites [1–3]. Strongly interacting species such as thiols can bind to noble metal surfaces and have been shown to influence reaction selectivity through various mechanisms (including active site selection, molecular recognition, and steric effects) [4]. However, species with intermediate or weak surface interactions can also interact with the metal surface and induce substantial reaction effects, especially when present at high concentrations. For example, adsorbed oxygenated aromatics and other biomass analogues have been shown to poison the metal catalyst surface by blocking sites, and varying coverages of furyl species have been implicated in driving different adsorption geometries and reactions [5,6]. Similarly, co-adsorbed solvent molecules such as water or ethanol can directly participate in reactions on the metal surface and have also been shown to indirectly influence reaction pathways through stabilization of key intermediates [7,8]. Computational approaches to improving catalytic reactions in the liquid phase continue to attract intense interest and dovetail with the increasing emphasis on the use of water as a solvent for green chemical reactions [9]. However, accurate modeling of aqueous phase chemistry is predicated on the understanding of adsorbate interactions in the near-surface environment; this necessitates experimental benchmarking of adsorption free energies from solution.

Despite deep relevance to catalytic reactions, experimental measurement of the interaction of organic molecules with metal surfaces as well as the resulting steady-state adsorbate coverage remains challenging. While the total adsorbed amount of very strongly bound adsorbates can be quantified through elemental analysis, [10,11], capturing the behavior of transiently bound species that adsorb through intermediate or weak surface interactions is challenging, particularly under conditions relevant to catalytic reactions. Even for strongly bound adsorbates, the apparent adsorbed amount can be difficult to interpret in the context of catalysis due to potential artifacts including multilayer formation or adsorption to the support. Sophisticated instrumentation and spectroscopic techniques have been employed in these efforts; for example, a combination of electrochemical techniques and X-ray spectroscopy has been used to successfully probe organic coverage and to extract adsorption energies [12]. In particular, cyclic voltammetry (CV) has been used to estimate the coverage of organics on Pt and Rh wires via charge changes in hydrogen underpotential deposition. These results were corroborated by X-ray Absorption Spectroscopy (XANES), which directly probed the hydrogen surface coverage on the Pt surface. However, both these techniques necessitate the application of a potential to the surface (and cycling over a range of potentials for CV) which may skew adsorption relative to an uncharged surface [13].

Here, we show the utility of self-propelled active particles for quantification of the affinity and apparent saturation coverage of adsorbates on a platinum surface under steady state reaction conditions. Active particles that convert chemical energy into motion can potentially be used in applications for colloids that can propel, sense, carry, and deliver cargo [14–16]. Sensing is a particularly attractive avenue as the active drift velocity or "swimming speed" of a variety of active particles has been shown to be sensitive to dissolved species [17]. Consequently, changes in the active velocity have been used as a sensing indicator and numerous studies have promoted the use of active particles as sensors for the solution viscosity and for pollutants such as heavy metal ions, nitrates, or organic species in solution [18,19]. In particular, metal catalyzed, peroxide-fueled active motion has been shown to be sensitive to thiolate species [20]. One of the most prevalent classes of active matter, Janus colloids with anisotropic metal deposition (typically on one half of the particle surface), move autonomously in H_2O_2 solutions due to asymmetry in the rates of catalytic peroxide decomposition across the particle [21]. The decomposition products create a concentration gradient behind the particle, propelling it directionally at speeds exceeding typical Brownian motion. Since the decomposition of H_2O_2 occurs on the metal surface, catalyst poisoning can disrupt the active motion. In fact, complete deactivation of Pt microjets was reported using micromolar concentrations of biological thiols [20]. This attenuation of active motion was directly attributed to the binding of thiols to the Pt surface, which blocked catalytic sites and inhibited the peroxide decomposition reaction.

We exploited the dependence of active motion on solute concentration to quantify adsorption on available metal surface sites. As a positive control, a strongly binding thiol was used to validate the technique, which was then applied to extract the binding affinity and final saturation coverage of both furfural, a commercially important biomass derivative with an intermediate-strength interaction with the metal surface, as well as the weakly interacting ethanol co-solvent. Moreover, the adsorption behavior of furfural and ethanol was analyzed at elevated temperatures to construct a series of adsorption isotherms, allowing for direct extraction of the enthalpy of adsorption (ΔH_{ads}). This approach combines key elements of active particle behavior to gain insights into catalysis and helps capture one of the most salient aspects of catalysis, i.e., the competitive *in situ* interactions of the reactant, competitive adsorbate, and metal surface under reaction conditions in an aqueous phase. Moreover, this approach is broadly applicable to adsorbates with a wide range of surface affinity, measures adsorption in a way that is directly relevant to catalytic activity and is experimentally accessible (necessitates only a microscope and utilizes minimal catalyst amounts).

2. Materials and Methods

Active Particle Synthesis

A suspension of 1 µm particles (carboxylate-modified polystyrene, fluorescent yellow-green, Sigma-Aldrich) were diluted to ~10^{-12} M in ethanol (anhydrous, 200 proof, Decon Labs) and were spin coated onto clean glass cover slips (22 x 22mm, No. 1.5, Ted Pella). The particle concentration of the suspension was adjusted to give a sub-monolayer of particles on the cover slip; 20 µl of the particle solution was spin coated at 2000 rpm onto each slip (15 slips total). The particles on the slips were then sputter-coated (Cressington 108Auto) with platinum (Pt) to deposit a 10 nm layer of Pt on the exposed particle hemisphere. The Pt layer thickness was monitored via an attached Cressington Thickness Monitor. The particles were liberated from the glass slide by sonication (2-3 min) and redispersed into 4 mL of water (high-performance liquid chromatography (HPLC)-grade, ≥99.9%, Fisher). The anisotropic metal deposition of the synthesized active particles was confirmed by drop-casting a small aliquot (~7 µl) of the active particle solution onto a holey carbon-coated copper grid (Ted Pella) and subsequent analysis via transmission electron microscopy (TEM) using a Tecnai ST20 operating at 200 kV. Representative TEM micrographs of the active particles (and unmodified particles as reference) are shown in the supporting information (Figure S1). To minimize photobleaching, bottles containing the active particle solution were wrapped in foil and stored at 3 °C. Before imaging, the solution was stirred vigorously using a vortex mixer and then sonicated for ~20 minutes to break up particle aggregates.

Imaging Particle Dynamics

Active and passive particle dynamics were monitored using a Nikon N-Storm microscope using a Hamamatsu ORCA-Flash4.0 V2 C11440 camera and a 100× oil immersion objective (NA: 1.45). The fluorescent particles were excited using a 561 laser line (Agilent Technologies MLC400B) and the emission light was passed through double-helix point spread function (DH-PSF) SPINDLE module (Double Helix LLC, Boulder).

Prior to imaging, 20 µl of hydrogen peroxide (30% w/w, Fisher) was added to 40 µl of the particle dispersion to form a 10% H_2O_2 solution (60 µl total volume). Imaging cells were constructed by attaching self-adhesive annular silicone spacers (SecureSeal spacers, 9mm diameter x 0.12 mm depth, Electron Microscopy Sciences) to cleaned glass slips (22 x 22mm, No. 1.5, Ted Pella); an aliquot (3 µl) of the H_2O_2 and particle solution was pipetted into the well formed by the spacer, and another glass slide was fixed on top to minimize ambient noise and evaporation. Since the properties of vicinal surfaces are known to impact active particle dynamics [22], all glass cover slips used as imaging supports were cleaned using piranha solution (1:3 mixture of 30% H_2O_2 and concentrated H_2SO_4) for at least 3 hours to remove possible contamination.

Multiple movies (3600 frames, acquisition time of 10 ms) at different fields of view were obtained of particles moving in the vicinity of a solid glass support surface. This process (mixing particles with H_2O_2, construction of imaging cell, and imaging) was repeated at least three times for each tested condition (corresponding to >50 colloids imaged). The duration between the initial mixing of the particle solution and H_2O_2 and the cessation of imaging was typically less than 10 minutes; this short time span coupled with the low particle concentration (~10^{-13} M) and reported kinetics for H_2O_2 decomposition [23] resulted in the H_2O_2 concentration remaining essentially constant during imaging (<1% decrease of H_2O_2 in 10 minutes). Passive dynamics were measured using similar procedures but without the addition of H_2O_2 (20 µl of HPLC-grade water were instead added to 40 µl of the particle solution to maintain a similar particle concentration between active and passive experiments and 3 µl aliquots of this solution were imaged).

Incubation of Active Particle Solution with Adsorbates

Adsorbate coverage on the metal surface of the particle was tuned by incubating varying concentrations of each adsorbate (1-thioglycerol (≥99.0%, Sigma-Aldrich), furfural (99%, Sigma-Aldrich), or ethanol (anhydrous, 200 proof, Decon Labs)) with the particle solution for at least two hours prior to imaging (total incubated volume of 150 µl). Immediately before imaging, 40 µl of the incubated adsorbate/particle solution was mixed with 20 µl of H_2O_2 and vigorously stirred before a 3 µl aliquot was pipetted onto the glass cover slip substrate of the imaging cell. Passive dynamics were imaged using an aliquot (3 µl) of the incubated solution pre-mixed with water (40 µl and 20 µl, respectively) instead of H_2O_2.

Inductively coupled plasma mass spectrometry (ICP-MS) was used to measure the amount of adsorbed thioglycerol on the Pt surface at different incubated concentrations. As the synthesis yield of the active particles was too limited (~1 mg) for quantitative ICP results, a well-characterized 5% Pt/Al_2O_3 catalyst (Sigma-Aldrich) was used as a proxy surface for the thioglycerol coverage measurement. Samples of Pt/Al_2O_3 (100 mg) were incubated at different thioglycerol concentrations that corresponded to the conditions used in the active particle experiments, rinsed three times with water to remove any weakly bound thiols, and finally dried under vacuum prior to ICP analysis.

Data Analysis

Particle trajectories (temporal x, y, and z localization) were generated from the movies using DH-TRAX™ software. The DH-PSF SPINDLE module converts the original Airy disk point spread function into two lobes; the lateral x and y positions were determined from the midpoint of these two lobes and the z position was determined from the relative azimuthal angle of the lobes using a calibration that maps angles to axial positions (Figure S2). The approximate x, y, and z precisions were 10 nm, 10 nm, and 20 nm, respectively [24].

Particle motion was quantified by calculating the time-averaged mean-square displacement (MSD) of the trajectories. The passive 2D translational diffusion coefficient D_T was first experimentally determined by fitting the MSD data (Δr^2) versus lag time Δt to expression (2) for passive particle dynamics exhibited in the absence of H_2O_2 at each tested solution composition (i.e., each measured adsorbate concentration).

$$\Delta r^2 = 4D_T\Delta t \qquad (1)$$

All measured D_T values (and associated rotational diffusion coefficients (D_R) and characteristic rotational time scales (τ_R)) are reported in Table S1. We note that the presence of thioglycerol and furfural (even at highest tested concentration of 100 mM) appeared to have no noticeable impact on the measured D_T; consequently, the same value of D_T (0.385 $\mu m^2/s$) is reported both for experiments using these molecules and for the experiments with no adsorbate present. Ethanol, however, had a noticeable impact on the measured D_T (likely due to the increasing viscosity of ethanol/water mixtures) and the corresponding D_T is reported for each ethanolic composition. Subsequently, these D_T values were used as a fixed parameter to extract the active particle drift velocity V from active experiments (H_2O_2 present) at the corresponding solution compositions using expression (3) [21].

$$\Delta r^2 = 4D_T\Delta t + V^2\,\Delta t^2 \qquad (2)$$

Since equation 2 is valid for short-time scales short compared to the characteristic time for rotational diffusion, only the first 11 data points were used for the fits to expressions 2 and 3 (corresponding to a lag time of 0.10 s). This time interval was appropriate to accurately determine the dynamic parameters since the characteristic time for particle rotation, $\tau_R = 1/D_R \approx 1.03$ s (where $D_R = 0.96$ rad^2/s is the rotational diffusion coefficient). All extracted velocities are detailed in the supporting information.

While all three Cartesian components of particle motion were experimentally measured using the DH-PSF, all analyses in this report use the motion in x and y plane. Several reasons motivated this choice. The active particles displayed a well-documented quasi-2D motion [25] near the interface and the inclusion of the z-component had a minimal impact on the analyses. Furthermore, since all particles were imaged near the solid-liquid interface the presence of the glass surface could potentially contribute to partial confinement in the z-direction. Finally, since the experimental precision in the x and y positions was substantially better than in the z-direction (by approximately a factor of two), the analysis of two-dimensional projected trajectories reduced artifacts due to localization error noise.

Effective adsorbate coverages were determined from the extracted velocities as described in the Results and Discussion (expression 1). The coverage plots were fit to the Langmuir isotherm adsorption given by:

$$\theta = \theta_{max} \frac{K_a C}{1+K_a C} \qquad (3)$$

where C is the adsorbate concentration, θ is the adsorbate coverage, θ_{max} is maximum saturation coverage and K_a is the affinity of each adsorbate to the catalyst surface. Expression (3) was linearized by plotting C/θ versus C, yielding a slope of $1/\theta_{max}$ and an intercept of $1/(\theta_{max} K_a)$ [26]. The error values given in the text represent the propagated standard error from the fit for each parameter.

Error bars for the particle velocity and coverage were computed by calculating the standard error of the drift velocity and subsequent uncertainty propagation, respectively.

The enthalpies of adsorption for furfural and ethanol were determined by analyzing the respective adsorption isotherms at three temperatures (294 K, 303 K, and 311 K). The particle solutions and H_2O_2, and glass slides substrates were all incubated at the elevated temperatures using an environmental chamber (Okolab Cage Incubator) that was also used to control the temperature of the particle solution during imaging. The fits to isotherms were used to derive the enthalpy of adsorption via the Clausius–Clapeyron approach [27]. To extract the enthalpy, the isotherms at different temperatures must be compared at the same coverage θ, which was not generally possible using experimentally measured data points. Since the data were well described by a Langmuir isotherm, the Langmuir expression (4) was inverted to provide a continuum of concentration and coverage data points using the best fit parameters for each experimental condition.

$$C = \frac{\theta}{K_a \theta_{max} + K_a \theta} \qquad (4)$$

Using the fitted Langmuir parameters, the enthalpy was evaluated as a function of C by plotting the natural log of the concentration values for a given coverage against the corresponding reciprocal temperature (ln(C) vs 1/T); the product of the slope of this relation and the gas constant R gives the enthalpy of adsorption. The enthalpy values presented in the main text show the values of enthalpy at 1% coverage for each adsorbate and the uncertainties for the extracted enthalpy values represent the standard error of the linear regression in the plot of ln C vs. 1/T.

Computational Methods

A brief description of the methodology and computational details can be found in the Supporting Information. Using our QM/MM FEP approach, we calculated the solvent effect on the adsorption free energy ($\Delta\Delta G_{ads}$) of furfural at low coverage conditions ($\Delta\Delta G_A^{gas\rightarrow liq}(\theta_A = 0)$) at 298 K to be 0.88±0.07 eV. To compare our computationally predicted solvent effect with the experiment, we employed the adsorption model from Nitta et al. [28] derived directly from statistical mechanics.

In the aqueous phase, both furfural and hydrogen peroxide can adsorb on the Pt surface, and therefore

$$\theta_* + \theta_B + n\theta_A = 1 \qquad (5)$$

where θ_A, θ_B, and θ_* are the fractional surface coverages of furfural, hydrogen peroxide, and the free site, respectively, and n represents the number of sites occupied by the furfural species.

This leads to the following equation for the liquid phase multicomponent adsorption isotherm (see the Supporting Information for a full derivation).

$$\theta_A = K_{ads,A}^{gas}(\theta_A = 0)K_{H,A}C_A\left(\frac{1-n\theta_A}{1+\gamma_B}\right)^n \exp\left[\frac{-\left\{\Delta\Delta G_A^{gas\rightarrow liq}(\theta_A=0)+\alpha_{A,A}^{liq}\theta_A\right\}}{RT}\right] \qquad (6)$$

Here, $K_{ads,A}^{gas}(\theta_A = 0)$ is the gas-phase adsorption equilibrium constant of furfural at low coverage, $K_{H,A}$ is the Henry's constant of furfural in water ($K_{H,A} = 5.13 \times 10^{-3}\ bar/M$ at 294 K) [29], C_A is the furfural concentration in the aqueous phase, γ_B is a lumped parameter that is the ratio of hydrogen peroxide derived species to the free site coverage (e.g., $\gamma_B = 0$ indicates that the surface contains only free and furfural occupied sites), $\alpha_{A,A}^{liq}$ signifies the lateral interaction strength between two adsorbed furfural molecules in the aqueous phase, R is the molar gas constant, T is the system temperature, and $\Delta\Delta G_{Ads}^{gas\rightarrow liq}(\theta_A = 0)$ which is defined as:

$$\Delta\Delta G_A^{gas\rightarrow liq} = \Delta G_{ads,A}^{g-l} - \Delta G_{ads,A}^{g} \qquad (7)$$

$$\Delta G_{ads,A}^{g-l} = \Delta G_{ads,A}^{l} + \Delta G_A^{solvation} \qquad (8)$$

Here, $\Delta G_{ads,A}^{l}$ and $\Delta G_{ads,A}^{g-l}$ are the adsorption free energies of furfural in the aqueous phase from its solvated state in solution and from its free state in the gas phase, respectively, $\Delta G_A^{solvation}$ is the solvation free energy of furfural which can be obtained from the Henry's constant at relevant temperatures, and $\Delta G_{ads,A}^{g}$ is the gas phase free energy of adsorption in the absence of any liquid in the fluid and adsorbed phases. In other words, $\Delta\Delta G^{gas\rightarrow liq}$ is ΔG for the reaction of moving a molecule A adsorbed on the Pt surface in the gas phase to a different water-covered Pt slab that ends with the adsorbate sandwiched between the Pt and the water, at low coverage.

A^{n*}(*gas*) + n*(*liq*) → A^{n*}(l*iq*) + n*(*gas*) (9)

3. Results and Discussion

Tracking Active and Passive Motion

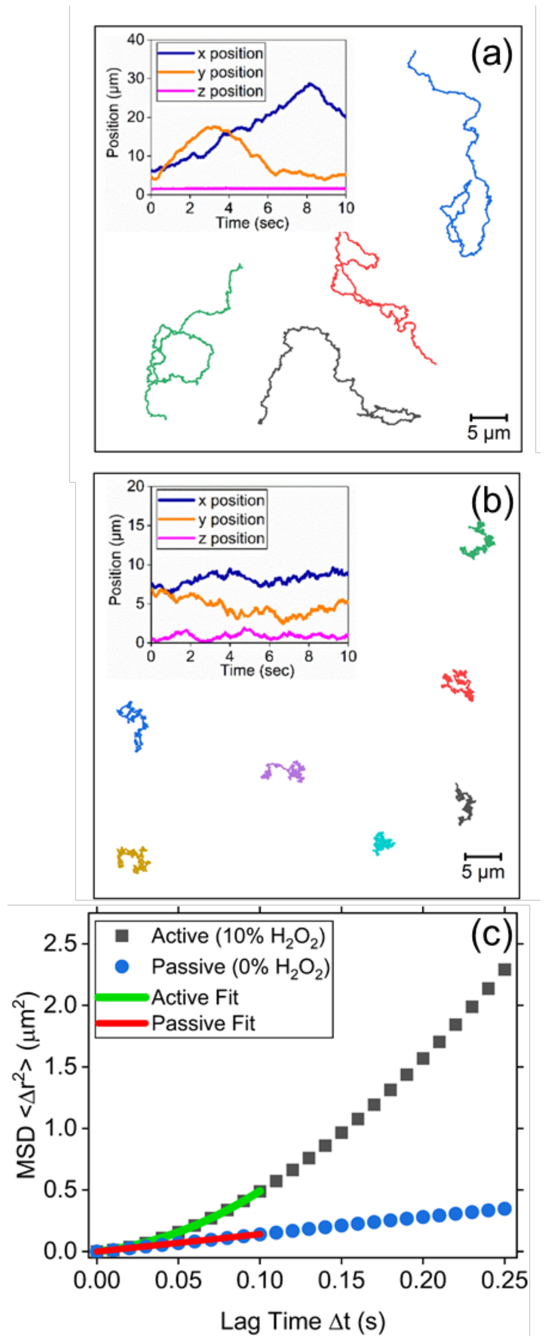

Figure 1. Representative 2D trajectories (10 seconds) for (a) particles in a 10% H_2O_2 solution exhibiting active motion and (b) particles with no fuel present exhibiting passive Brownian motion. Insets show representative Cartesian coordinate time series data, where the z-direction is normal to the imaging support surface. (c) The calculated mean-square displacement (MSD) curves for representative active and passive particle trajectories and the corresponding fits ($\Delta r^2 = 4\ D_T\ \Delta t + V^2\ \Delta t^2$ for the active case, $\Delta r^2 = 4D_T\Delta t$ for the passive case) to determine D_T and V (0.385 um^2/s and 5.92 um/s, respectively).

Active Janus particles (1 µm diameter) with Pt deposited on approximately one-half of the particle were synthesized and their dynamics were imaged near to the surface of the glass substrate. In a 10% H_2O_2 solution, the particles displayed clear activity and explored significantly larger areas compared to the passive case with no H_2O_2 present (Figure 1a and b). (Also see movies S1 and S2 for representative active and passive motion, respectively). While particle rotation (with an estimated $\tau_R \approx 1.1$ s) gradually randomized the direction of propulsion (explaining the lack of purely ballistic straight trajectories), the active trajectories displayed more persistent directional motion compared to the passive case. MSD analysis is a powerful tool to distinguish the degree of active vs Brownian motion and to quantify the active particle velocity. As shown in Figure 1c, the MSD for active particles exhibited a characteristic ballistic-like regime at short lag times that scales as time squared. While a transition to an apparent Brownian regime with a power law scaling of unity occurs at longer times, the short lag time regime is the most important for determining the particle velocity. The timescale of the transition to the asymptotic apparent Brownian regime was associated with rotational diffusion of the particle and the effective diffusion coefficient in that regime results from the combined effects of thermal and active motion in the presence of rapid rotation. To extract relevant parameters such as the translational diffusion coefficient D_T and the drift velocity V, the short lag time regimes of the MSD curves were fit to expressions for passive and active motion (described in detail in Materials and Methods). Briefly, the first 11 points of the passive MSD curve were fit to $\Delta r^2 = 4D_T\Delta t$ to extract D_T, in this case 0.351 um^2/s. This value of D_T was then used as a fixed parameter in the expression for active motion ($\Delta r^2 = 4D_T\Delta t + V^2 \Delta t^2$) to extract the value of V: 5.92 um/s.

The active motion also manifested the expected quasi-2D motion [25] near the substrate, as shown by the lack of fluctuations in the z-direction. This effect is hypothesized to result from a coupling of hydrodynamic forces between the particle and substrate, and typically causes active particles to move parallel to solid substrates [30]. Analysis of the particle z-position (insets to Figure 1) clearly demonstrated this phenomenon: throughout the entire length of their trajectories, active particles maintained a nearly constant separation from the wall. In contrast, the z-position of passive particles exhibited the expected Brownian fluctuations. Interestingly, as the particle activity was systematically attenuated by the addition of adsorbate molecules, analysis of the z-position increasingly resembled the passive fluctuations (Figure S3), suggesting that inhibition of the active mechanism directly perturbed the quasi-2D active motion.

Adsorbate-mediated attenuation of active motion

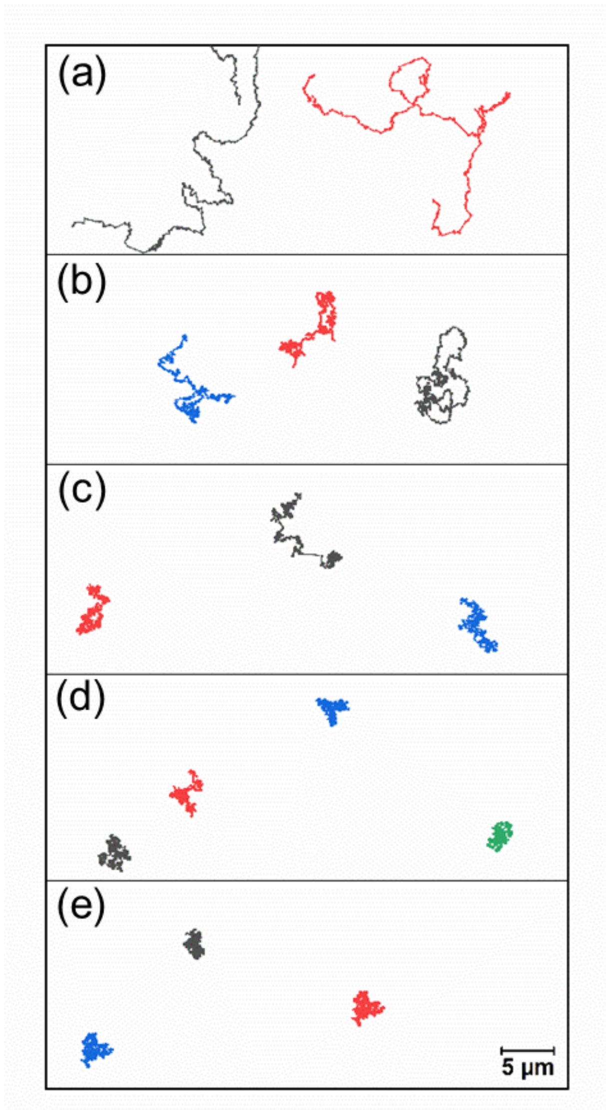

Figure 2. Representative 2D trajectories (10 seconds) showing the systematic attenuation of active particle motion in a 10% H_2O_2 solution due to increasing thioglycerol concentration: (a) no thioglycerol present, (b) 0.05 mM thioglycerol, (c) 0.1 mM thioglycerol, and (d) 2 mM thioglycerol. Panel (e) shows passive motion (no H_2O_2) for reference.

Thioglycerol contains a sulfhydryl group and consequently is expected to interact strongly with Pt through the thiol moiety [31]. When the particles were incubated in a 0.05 mM solution of thioglycerol, the observed trajectories explored significantly less area than the case with no thiol present (Figure 2a and b). This effect was also apparent in the MSD curves of the thiol-incubated particles: the ballistic regime became less pronounced, and the observed activity was nearly halved (Figure 3a). Doubling the thioglycerol concentration to 0.1 mM led to a further sharp reduction in the activity and ballistic regime, a trend that continued when the thioglycerol concentration was increased to 0.2 mM and 1 mM. Finally, at 2 mM thioglycerol, the particles displayed no observable directional motion and the trajectories closely resembled that of passive particles in the absence of H_2O_2 fuel (Figure 2d). Moreover, MSD analysis of the particle motion with 2 mM thioglycerol (Figure 3a) displayed a straight line that overlayed the data obtained from the passive experiments (in the absence of fuel), suggesting the saturation of the surface by thioglycerol that functionally eliminated access of H_2O_2 to the metal sites.

Furfural was used to further probe the influence of the adsorbate-metal interaction on particle dynamics. Widely studied as an intermediate in biomass refining, furfural can interact with Pt through both its aromatic ring as well as the carbonyl functionality and was expected to exhibit substantial interactions with the Pt surface, although significantly weaker than that of the thiol [32]. Qualitatively similar to thioglycerol (though at significantly higher concentrations), incubation of 1 mM furfural with the particles led to a reduction in active motion and further increased furfural concentrations resulted in progressive attenuation of active motion (Figure 3b). Interestingly, the MSD curves at the highest furfural concentrations (10 and 100 mM) did not collapse onto the passive case as occurred with thioglycerol. Rather, the behavior at high furfural concentration still exhibited a noticeable ballistic regime and enhanced active motion relative to passive Brownian particles, suggesting that even under conditions where furfural adsorption had apparently saturated, the Pt surface was not completely deactivated.

Finally, to probe the effect of a weakly adsorbing species on the particle motion, varying concentrations of ethanol were incubated with the particle solution. While ethanol can interact with Pt through the oxygen moiety, the expected binding strength is weak [33,34] and the concentration of ethanol required to induce observable changes in particle dynamics was 0.17 M (1% ethanol by volume), more than three orders of magnitude greater than that required for thioglycerol or furfural. While increasing amounts of ethanol (Figure 2c) in solution attenuated the activity to some extent, as for furfural, the active motion was not fully quenched. Indeed, the particles retained more than half of the original active motion in a solution containing 1.9 M ethanol. We note that at such high concentrations of ethanol, the liquid phase viscosity was measurably greater [35]. As a result, the MSD of passive Brownian particles 1.9 M ethanol solution was slightly lower than that of passive particles in the absence of ethanol (dashed lines in Figure 2c show this range of passive dynamics), but this small effect did not substantially influence the analysis (detailed in the supporting information and Figure S4). As with thioglycerol and furfural, a direct attenuation of the drift velocity was the dominant factor; however, the degree of the velocity attenuation was both less severe and required much higher relative concentrations of ethanol compared to furfural and thioglycerol adsorption.

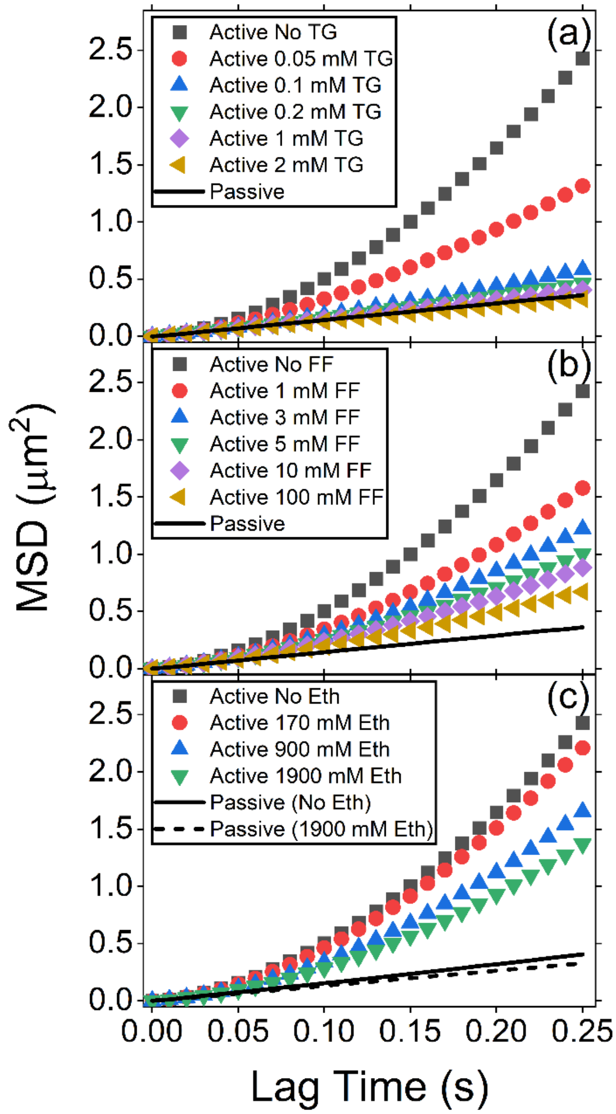

Figure 3. Mean square displacement vs lag time for motion exhibited by the particles at 294 K at different concentrations of adsorbates (a) thioglycerol (TG), (b) furfural (FF), and (c) ethanol (Eth). Solid lines show passive motion with no fuel added and the dashed line in (c) shows the reduced passive activity due to the viscosity of the 1.9 M ethanol solution.

Quantitative analysis of active motion and apparent surface coverage

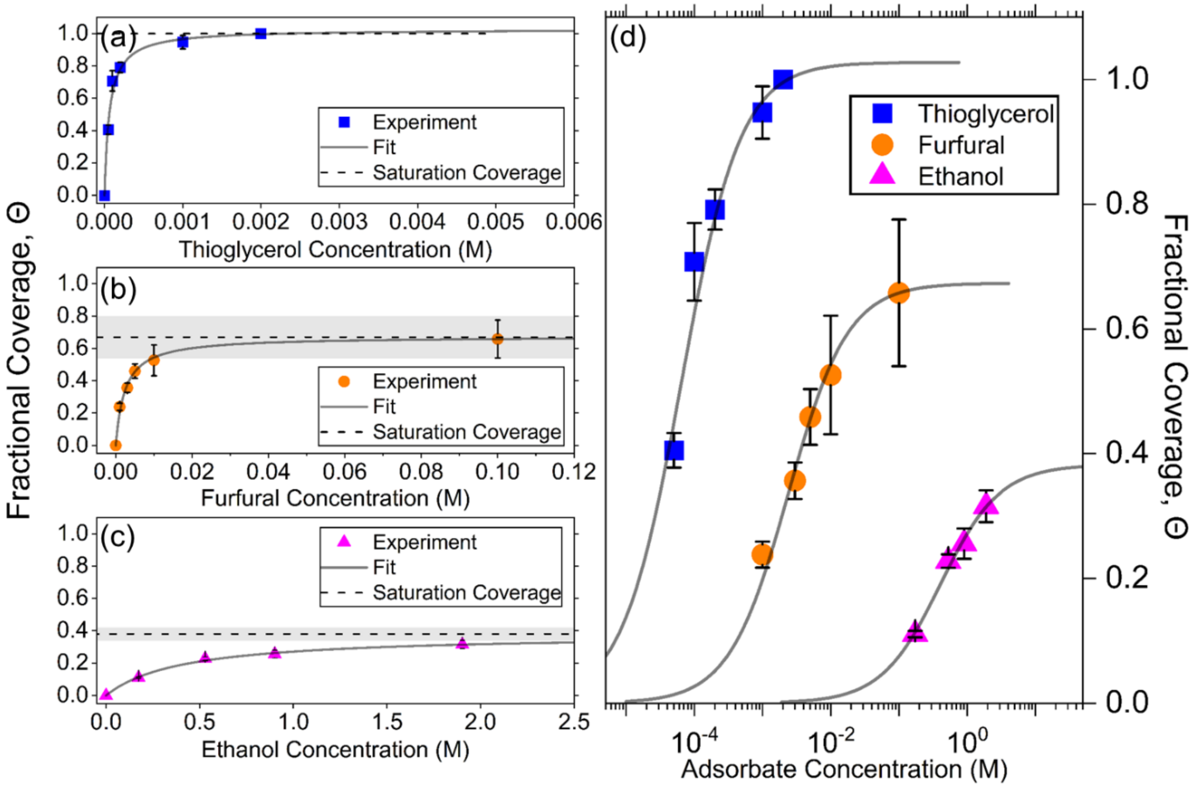

Figure 4. Apparent adsorption isotherms for (a) thioglycerol, (b) furfural, and (c) ethanol at 294 K. Symbols represent experimental data, solid lines show the calculated fit to a Langmuir isotherm, and the dashed lines and shaded area show the maximum saturation coverage and associated uncertainty, respectively. (d) The data from a-c on a semi-logarithmic scale

To quantitatively characterize the degree of active motion reduction induced by the adsorbates, the particle drift velocity at each adsorbate condition was first extracted from the MSD data and the apparent fractional surface coverage (θ) was inferred by comparing the observed velocity at a given adsorbate concentration (V) with the particle velocity in the absence of adsorbate (V_0) using the following equation:

$$\theta = 1 - \frac{V}{V_0} \qquad (10)$$

While the parameter θ is termed fractional adsorbate coverage, it is more accurate to say that it measures the extent to which H_2O_2 decomposition is blocked. While this blocking plausibly takes the form of the adsorbate covering the exposed metal surface sites, it is possible other mechanisms may also contribute. Moreover, the equation assumes the velocity is proportional to the fraction of empty Pt sites and that different types of Pt sites (such as (111)-terraces and (110) and (100)-steps) have similar contributions to the observed velocity. While more subtle effects (such as adsorbates tuning the activity of some sites) are not currently known for this system, they could result in second order corrections to the calculated coverages. The effective adsorbate coverage (or more precisely, the ability of each adsorbate to block H_2O_2 access to the surface) was plotted against the adsorbate concentration (Figure 4); the values of drift velocity and apparent coverage are collected in the Supporting Information (Table S2). As expected from the behavior of the MSD, thioglycerol rapidly saturated the surface and complete apparent coverage was achieved at 2 mM thioglycerol. Furfural, however, did not fully block H_2O_2 access to the surface and saturation of active motion reduction instead occurred at a maximum apparent coverage of approximately 0.67. Ethanol (at much higher concentrations relative to thioglycerol and furfural) similarly saturated at an effective coverage of less than 0.5. To better quantify these phenomena, each adsorbate coverage plot was linearized (Figure S5) and fitted to a Langmuir adsorption isotherm, allowing for extraction of the apparent maximum saturation coverage (θ_{max}) and surface affinity of each adsorbate (K_a) (Table 1).

Table 1: Extracted Coverage Parameters at 294 K

	Thioglycerol	**Furfural**	**Ethanol**
Affinity K_a *(mM^{-1})*	15.5 ± 4.3	0.42 ± 0.07	0.0025 ± 2x10^{-4}
Maximum Apparent Coverage θ_{max}	1.027 ± 0.001	0.67 ± 0.13	0.38 ± 0.04

As expected, the affinity of thioglycerol towards the surface was the highest of the measured adsorbates, followed by furfural and then ethanol. We note that these extracted affinities span more than four orders of magnitude, showcasing the broad applicability of this technique. Interestingly, the extracted maximum coverage appeared to trend with the affinity of each adsorbate, with the strongly interacting thioglycerol saturating the surface and fully deactivating the particle. The maximum adsorption of furfural, however, blocked only 0.67 of the metal surface while the weakly interacting ethanol occluded only 0.38 of the surface at high concentrations, according to the fits. While saturation coverage should approach unity in the limit of high adsorbate concentration, the presence of some sites with much lower affinities towards the adsorbates and/or the binding of adsorbates in different configurations could explain an apparent saturation at lower concentrations and coverages. Moreover, the presence of the nearly constant 10% H_2O_2 precludes the possibility of accessing the limiting case behavior of infinite adsorbate coverage, particularly for ethanol. We note that high amounts of ethanol in solution can impact properties including viscosity and oxygen solubility [35,36], therefore; access to the highly concentrated ethanol regime was limited to minimize the effect of the changing fluid properties.

To compare this coverage measurement technique with conventional methods, the total amount of adsorbed thiol on a proxy supported Pt catalyst was directly measured using inductively coupled plasma (ICP) analysis of sulfur composition. As the procedure to synthesize the active particles had a limited yield, a commercial supported Pt catalyst (5% Pt on alumina) was used as a proxy for the ICP measurements. The ICP results for adsorbed sulfur at low thiol concentrations (Figure S6a) showed good agreement with the effective coverage results obtained from the active particles, with similar values of surface affinity in this regime. Interestingly, however, the adsorbed thiol as measured by ICP was not well-described by a Langmuir isotherm and the linearized data (Figure S6b) appeared to exhibit two regimes: a higher affinity regime at lower concentrations (<1mM) and reduced affinity at higher concentrations (>1mM). This behavior was consistent with two populations of adsorption sites, with the high affinity adsorption presumably on Pt surface sites, and the second low affinity regime on other non-catalytic sites on the particle. The ICP measured high thiol affinity at low concentrations (<1 mM) in good agreement with the thiol affinity obtained in the same low concentration regime via the active particle experiments (22 ± 8 and 15.5 ± 4.3 mM^{-1}, respectively), consistent with the interpretation that thiol chemisorption attenuates the active motion until full monolayer coverage is achieved on the Pt surface. At higher concentrations, the thiol presumably continues to adsorb with lower affinity (2 ± 1 mM^{-1}) via physisorption to the alumina support or by multilayer formation. (Such additional adsorption to non-active sites is consistent with the anomalously high apparent value of thiol molecules per Pt surface area obtained from ICP measurements in the high thiol concentration regime, further detailed in the Supporting Information.) In contrast, the attenuation of active particle motion is specifically sensitive to coverage of the active sites and is consequently largely insensitive to any further adsorption to non-catalytic sites on the active particle. ICP analysis (and other types of elemental analysis), on the other hand, non-specifically measures the amount of adsorbed thiol on the entire supported catalyst sample, including material that is adsorbed to inactive sites or underlying adsorbate layers.

Enthalpy of Adsorption

The enthalpies of adsorption for furfural and ethanol were determined by analyzing isotherms at three temperatures: 294 K, 303 K, and 311 K (Figure 5, isotherm parameters collected in Table S3). Since the isosteric enthalpy of adsorption can be temperature-dependent, all three isotherms were measured with a total Δ*T* of less than 20 K to avoid introducing artifacts [27].

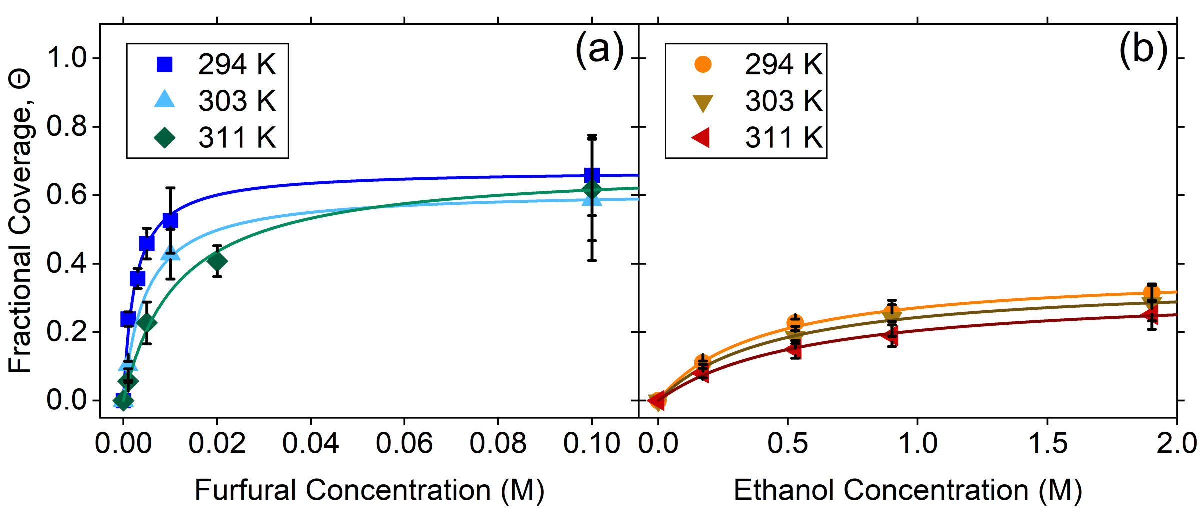

Figure 5. Apparent isotherms as a function of temperature for (a) furfural and (b) ethanol. Lines show isotherm fits (equation 4) to each isotherm. Isotherms with a common logarithmic scale given in Figure S7.

Per the van't Hoff equation, the isotherm fits (equation 4, extracted parameters collected in Table S2) were used to compare adsorbate concentration at the same coverage; the natural log of these concentration values were then plotted against the reciprocal corresponding temperatures to extract the enthalpy of adsorption (Table 2). The extracted enthalpy values were relatively stable over the coverage range (with increasing deviation from the norm as the surfaces approached saturation, Figure S8).

Table 2: Aqueous-Phase Enthalpy of Adsorption for Furfural and Ethanol

Adsorbate	ΔH_{ads} (kJ mol^{-1})*
Furfural	69 ± 4
Ethanol	23 ± 5

*values are for aqueous organic adsorbing onto Pt surface (all in water)

Intense recent interest in thermodynamics at the solid-liquid interface has revealed a profound effect induced by solvent molecules on the energetics of the adsorption process. Importantly, the presence of solvent can cause large decreases in heats of adsorption versus the gas phase, a phenomenon attributed to strong solvation of the organic and Pt surface [37]. We note that the measured values in Table 2 are for the strongest binding sites as more weaker-binding sites were likely not populated in the concentration regimes accessed in this study. The enthalpy of adsorption of furfural was also investigated using the method described in [13] (detailed in supporting information, values collected in Table S4). Interestingly, the extracted enthalpy of adsorption of the gas-phase furfural showed good agreement with the aqueous-phase enthalpy of adsorption (-71.5 and -69 kJ mol^{-1}, respectively). While this measured enthalpy is larger than that measured by complementary techniques [13], it is possible that the presence of H_2O_2 in this work and possible different solvation compared to neat water may help explain the discrepancy or that different adsorption geometries of furfural (flat-lying vs tilted) are being measured by the different techniques.

Computational Insights into the Adsorption of Furfural in Liquid Water

A full description of the thermodynamic cycle employed to compute the solvent effect on the adsorption free energy of furfural can be found in our upcoming publication [x]. A brief description of the methodology and computational details can be found in the supporting information. Figure S9 illustrates the average free energy profile for the desorption of a furfural molecule over Pt terrace sites at 298 K. We employed density functional theory calculations to compute the adsorption free energy of furfural over Pt terrace sites in the gas phase (at 294 K) and found the stable adsorption mode of furfural over the Pt(111) surface to be flat lying on the fcc hollow site (Figure S10), which agrees with other experimental and computational observations [38,39]. The free energy of adsorption at 294 K (ΔG_A^{gas}) was found to be

-121.75 kJ/mol. We then fitted our experimental observations at 294 K to Equation 7 for physically meaningful n and γ_B values to extract $\Delta\Delta G_A^{gas\rightarrow liq}(\theta_A = 0)$ and $\alpha_{A,A}^{liq}$.

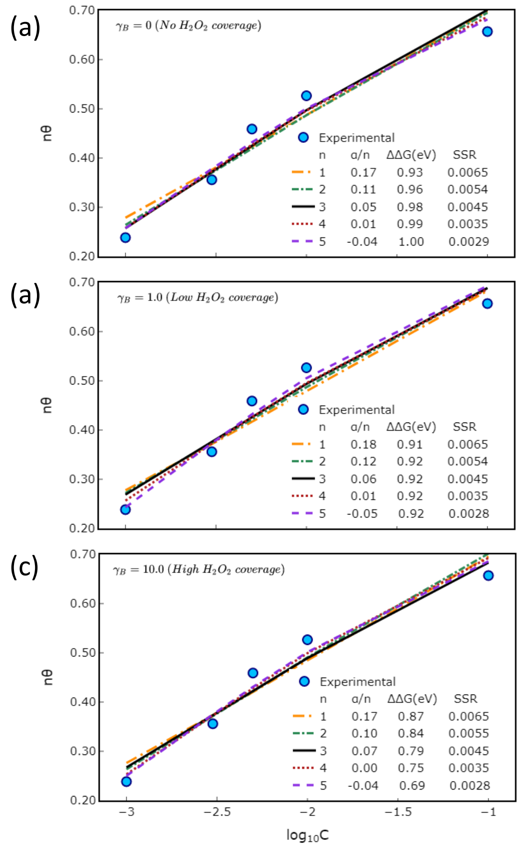

Figure 6. Fits of adsorption isotherms for aqueous phase furfural adsorption over Pt terrace sites at 294 K (assuming the enthalpy of adsorption in the gas phase is that from DFT for Pt terrace sites). The experimental data are displayed in blue markers and are fitted to the isotherm equation (Equation 7) assuming (a) no H_2O_2 coverage ($\gamma_B = 0$), (b) low H_2O_2 coverage ($\gamma_B = 1.0$), and (c) high H_2O_2 coverage ($\gamma_B = 10.0$). For each number of occupied metal sites by furfural, n, the figure displays the lateral interaction parameter between adsorbed furfural molecules, $\alpha_{A,A}^{liq}/n$ (symbolized as α/n, units of eV), the aqueous phase effect on the low coverage adsorption free energy of furfural, $\Delta\Delta G_A^{gas\rightarrow liq}(\theta_A = 0)$ (symbolized as $\Delta\Delta G$), and the sum of squared residuals (SSR) which shows the goodness of fit.

Figure 6 exhibits the best fits of the experimental observations at different hydrogen peroxide coverage approximations. In the zero hydrogen peroxide coverage approximation (Figure 6a) and for different numbers of furfural adsorption sites, the predicted $\Delta\Delta G_A^{gas\rightarrow liq}(\theta_A = 0)$ ranged from 0.93-1.00 eV which is in good agreement with our calculated solvent effect on the adsorption free energy (0.88±0.07 eV). Increasing γ_B to 1 (low H_2O_2 coverage, Figure 6b) changed $\Delta\Delta G_{ads}$ by less than 0.10 eV, such that the predicted solvent effect on the adsorption free energy was still within 0.10 eV of our computational prediction. Only at γ_B =10 (high H_2O_2 coverage, Figure 6c), i.e., where the coverage of H_2O_2 and its derivatives was 10 times as large as the free site coverage, did we observe significant deviations (~0.30 eV) between experimental and computational predictions of the solvent effects. In the experimental work, we employed a 10% H_2O_2 solution which suggests a low H_2O_2 coverage (γ_B < 1.0), resulting in a good quantitative agreement between the experimentally predicted $\Delta\Delta G_A^{gas\rightarrow liq}(\theta_A = 0)$ and the computational one.

Mechanism for Adsorbate-Mediated Activity Reduction

The likely mechanism for adsorbate-induced activity attenuation is the physical blockage of access of H_2O_2 to the metal sites. Sputtered Pt surfaces are crystalline with a face-centered cubic lattice [40]. Accordingly, the large Pt domain sizes of the sputtered film likely correspond largely to terrace sites [41]. Thiol adsorption is well-characterized and predominately occurs in threefold hollow terrace sites of the metal surface [31]. Direct measurement of sulfur content on a proxy Pt surface using ICP (Figure S6) showed thiol adsorption at < 1 mM concentrations with a comparable affinity to that determined by the attenuation of active motion, supporting the hypothesis that thiol adsorption on metal terrace sites directly contributes to the attenuation of active particle motion. Accordingly, at 2 mM thioglycerol concentration, the complete deactivation of the particles can be attributed to full occupation of the active Pt sites by a monolayer of strongly bound thioglycerol molecules that fully obstructed H_2O_2 access to the Pt surface. Physical occlusion of the Pt active sites is further supported by DFT calculations that suggest H_2O_2 decomposition primarily occurs on terrace sites of Pt catalyst facets, the same area where thioglycerol is also predicted to primarily bind [42]. Occlusion of H_2O_2 access to Pt sites by furfural and ethanol is also the hypothesized mechanism for the observed activity attenuation by these adsorbates. Interestingly, however, since the observed maximum apparent coverages were incomplete — 0.67 and 0.38 for furfural and ethanol, respectively — access of H_2O_2 to the surface was apparently not fully eliminated in either case despite the higher concentrations used and the ample abundance of adsorbate. We propose two possible explanations for the apparent saturation at lower coverages. First, adsorbates such as furfural are known to bind in different configurations depending on local coverage and site availability. At low coverage, furfural and similar adsorbates such as benzyl alcohol have been found to adsorb on Pt(111) and Pd(111) surfaces in a flat-lying, multidentate configuration (Figure S10) [38,43]. As coverage increases, the surface becomes populated with a more weakly adsorbed, “upright” state [44,45]. Over the concentration range explored here, it may be that only the flat-lying state is probed. Alternatively, multiple types of Pt sites may exist on the Pt surface and the observed maximum coverage of less than unity may be attributed to saturation of only a subset of the total sites. For example, while both terrace and edge sites have been implicated in H_2O_2 reactivity [42], edge sites are unlikely to foster favorable planar furfural adsorption geometry. Thus, the observed plateau in coverage may be due to the saturation of the active sites to which the adsorbate has the highest affinity. While continued adsorption and blockage of sites with much reduced affinity may occur at higher concentrations, the significantly lower affinity of the adsorbate to these sites results in overall negligible continued blockage of H_2O_2 decomposition and the observed saturation plateau of less than unity. We note that a similar saturation in furfural coverage on Pt of ~85% was also observed by Akinola et al. [13] using the hydrogen uptake method. While the apparent equilibrium constant was larger than that observed in this work (possibly due to free energy differences resulting from differences in applied potential and pH between techniques), the shared observation of a plateau of less than one in saturation coverage suggests that adsorbed furfural is not able to completely occlude the Pt surface. Moreover, in the aqueous milieu, competition with water or peroxide may be significant and competitive dynamic exchange between H_2O/H_2O_2 and the weakly-bound adsorbates may occur in the near-surface environment, helping to depress the maximum saturation coverage to less than unity even at relatively high adsorbate concentrations. Adsorption of solute molecules onto metal surfaces has large implications in catalysis and important parameters of this process can be captured using active particles, including the impact of multiple populations of active sites and competitive binding of the solvent on the apparent coverage.

4. Conclusion

In this study, we demonstrated the utility of active particles as a probe of metal surface-adsorbate interactions. For a several adsorbates (ranging from strongly interacting thiols to weakly interacting ethanol) the observed particle dynamics were used to extract both the surface affinity of each adsorbate and the respective apparent saturation maximum coverage in the presence of the hydrogen peroxide reactant. Strongly interacting thioglycerol fully occluded access of H_2O_2 to the metal surface and completely deactivated the particles. Saturation of the metal surface with furfural and ethanol, however, did not fully block the surface and instead resulted in maximum fractional coverages of 0.67 and 0.38, respectively. Furthermore, isotherms at elevated temperatures allowed for direct extraction of the aqueous enthalpy of adsorption for furfural and ethanol ($-\Delta H_{ads}$ values of 69 and 23 kJ mol^{-1}, respectively) and computational predictions of furfural adsorption showed quantitative agreement with the experimental results. We note that the adsorption enthalpy is both salient to catalysis and traditionally difficult to accurately measure in the aqueous phase. The active particle technique is effective over a wide range of adsorbate concentrations (nearly 4 orders of magnitude) and accurately captures in situ phenomena that are directly relevant to catalysis. Moreover, the technique requires only a microscope equipped with a camera and utilizes very small volumes and amounts of catalyst, potentially making it amenable to multiplexed experimental design for large-scale screening experiments. This work represents a new multidisciplinary paradigm for catalysis research and showcases the utility of active particle dynamics to uniquely elucidate key fundamental catalysis questions.

Associated Content

Supporting Information

TEM micrographs of the particles; DH-PSF images at different axial (z) positions; collected values for D_T, D_R, and T_R; detailed computational methods; evolution of z-position behavior; simulated active motion at higher viscosities; extracted velocities and apparent coverages; linearized Langmuir isotherms; ; sulfur coverage measured via ICP; isotherm parameters; extracted enthalpy ΔH_{ads} as a function of coverage and DFT-predicted furfural adsorption geometry as specified in the text

Movie S1: Representative active motion in a 10% H_2O_2 solution near the glass substrate

Movie S2: Representative passive motion (no H_2O_2 present) near the glass substrate

Author Information

Corresponding Author

Daniel K. Schwartz - *Department of Chemical and Biological Engineering, University of Colorado, Boulder, Colorado 80309, United States*

E-mail: *daniel.schwartz@colorado.edu*

Authors

Benjamin Greydanus- *Department of Chemical and Biological Engineering, University of Colorado, Boulder, Colorado 80309, United States*

Mohammad Saleheen - *Department of Chemical Engineering, University of South Carolina, 301 Main Street, Columbia, South Carolina 29208, United States*

Haichao Wu- *Department of Chemical and Biological Engineering, University of Colorado, Boulder, Colorado 80309, United States*

Andreas Heyden - *Department of Chemical Engineering, University of South Carolina, 301 Main Street, Columbia, South Carolina 29208, United States*

J. Will Medlin - *Department of Chemical and Biological Engineering, University of Colorado, Boulder, Colorado 80309, United States*

Notes

The authors declare no competing financial interest

Acknowledgments

This work was supported by the Department of Energy, Office of Science, Basic Energy Sciences Program, Chemical Sciences, Geosciences, and Biosciences Division [grant no. DE- SC0005239]. The imaging work was performed at the BioFrontiers Institute Advanced Light Microscopy Core and microscopy was performed on a Nikon Ti-E microscope supported by the Howard Hughes Medical Institute. This research was also supported in part by the Colorado Shared Instrumentation in Nanofabrication and Characterization (COSINC) and the CU Facility for Electron Microscopy of Materials (CUFEMM). B.G. acknowledges the Graduate Assistance in Areas of National Need Fellowship and the Department of Education for financial assistance. MS and AH acknowledge financial support from the U.S. Department of Energy, Office of Basic Energy Science, Catalysis Science program under Award DE-SC0007167.

References

[1] B.N. Zope, D.D. Hibbitts, M. Neurock, R.J. Davis, Reactivity of the gold/water interface during selective oxidation catalysis, Science (80-.). 330 (2010) 74–78. https://doi.org/10.1126/science.1195055.

[2] P. Hao, D.K. Schwartz, J.W. Medlin, Effect of Surface Hydrophobicity of Pd/Al2O3 on Vanillin Hydrodeoxygenation in a Water/Oil System, ACS Catal. 8 (2018) 11165–11173. https://doi.org/10.1021/acscatal.8b03141.

[3] B. Greydanus, D.K. Schwartz, J.W. Medlin, Controlling Catalyst-Phase Selectivity in Complex Mixtures with Amphiphilic Janus Particles, ACS Appl. Mater. Interfaces. 12 (2020) 2338–2345. https://doi.org/10.1021/acsami.9b16957.

[4] C.A. Schoenbaum, D.K. Schwartz, J.W. Medlin, Controlling the surface environment of heterogeneous catalysts using self-assembled monolayers, Acc. Chem. Res. 47 (2014) 1438–1445. https://doi.org/10.1021/ar500029y.

[5] M. Besson, P. Gallezot, Deactivation of metal catalysts in liquid phase organic reactions, Catal. Today. 81 (2003) 547–559. https://doi.org/10.1016/S0920-5861(03)00153-6.

[6] L.O. Mark, A.H. Jenkins, H. Heinz, J.W. Medlin, Furfuryl alcohol deoxygenation, decarbonylation, and ring-opening on Pt(111), Surf. Sci. 677 (2018) 333–340. https://doi.org/10.1016/j.susc.2018.07.001.

[7] Z. Zhao, R. Bababrik, W. Xue, Y. Li, N.M. Briggs, D.T. Nguyen, U. Nguyen, S.P. Crossley, S. Wang, B. Wang, D.E. Resasco, Solvent-mediated charge separation drives alternative hydrogenation path of furanics in liquid water, Nat. Catal. 2 (2019) 431–436. https://doi.org/10.1038/s41929-019-0257-z.

[8] P.J. Dyson, P.G. Jessop, Solvent effects in catalysis: Rational improvements of catalysts: Via manipulation of solvent interactions, Catal. Sci. Technol. 6 (2016) 3302–3316. https://doi.org/10.1039/c5cy02197a.

[9] M. Saleheen, A. Heyden, Liquid-Phase Modeling in Heterogeneous Catalysis, ACS Catal. 8 (2018) 2188–2194. https://doi.org/10.1021/acscatal.7b04367.

[10] P. Hao, S. Pylypenko, D.K. Schwartz, J.W. Medlin, Application of thiolate self-assembled monolayers in selective alcohol oxidation for suppression of Pd catalyst deactivation, J. Catal. 344 (2016) 722–728. https://doi.org/10.1016/j.jcat.2016.08.023.

[11] H. Hinterwirth, S. Kappel, T. Waitz, T. Prohaska, W. Lindner, M. Lämmerhofer, Quantifying thiol ligand density of self-assembled monolayers on gold nanoparticles by inductively coupled plasma-mass spectrometry, ACS Nano. 7 (2013) 1129–1136. https://doi.org/10.1021/nn306024a.

[12] N. Singh, U. Sanyal, J.L. Fulton, O.Y. Gutiérrez, J.A. Lercher, C.T. Campbell, Quantifying Adsorption of Organic Molecules on Platinum in Aqueous Phase by Hydrogen Site Blocking and in Situ X-ray Absorption Spectroscopy, ACS Catal. 9 (2019) 6869–6881. https://doi.org/10.1021/acscatal.9b01415.

[13] J. Akinola, I. Barth, B.R. Goldsmith, N. Singh, Adsorption Energies of Oxygenated Aromatics and Organics on Rhodium and Platinum in Aqueous Phase, ACS Catal. 10 (2020) 4929–4941. https://doi.org/10.1021/acscatal.0c00803.

[14] X. Chen, C. Zhou, W. Wang, Colloidal Motors 101: A Beginner's Guide to Colloidal Motor Research, Chem. - An Asian J. 14 (2019) 2388–2405. https://doi.org/10.1002/asia.201900377.

[15] S.J. Ebbens, J.R. Howse, In pursuit of propulsion at the nanoscale, Soft Matter. 6 (2010) 726–738. https://doi.org/10.1039/b918598d.

[16] H. Wu, B. Greydanus, D.K. Schwartz, Mechanisms of transport enhancement for self-propelled nanoswimmers in a porous matrix, Proc. Natl. Acad. Sci. U. S. A. 118 (2021) 1–8. https://doi.org/10.1073/pnas.2101807118.

[17] M. Pacheco, M. Ángel López, B. Jurado-Sánchez, A. Escarpa, Self-propelled micromachines for analytical sensing: a critical review, Anal. Bioanal. Chem. 131 (2019) 12082–12083. https://doi.org/10.1021/ja905142q.

[18] L. Wang, T. Li, L. Li, J. Wang, W. Song, G. Zhang, Microrocket Based Viscometer, ECS J. Solid State Sci. Technol. 4 (2015) S3020–S3023. https://doi.org/10.1149/2.0051510jss.

[19] J. Parmar, D. Vilela, K. Villa, J. Wang, S. Sánchez, Micro- and Nanomotors as Active Environmental Microcleaners and Sensors, J. Am. Chem. Soc. 140 (2018) 9317–9331. https://doi.org/10.1021/jacs.8b05762.

[20] G. Zhao, S. Sanchez, O.G. Schmidt, M. Pumera, Poisoning of bubble propelled catalytic micromotors: The chemical environment matters, Nanoscale. 5 (2013) 2909–2914. https://doi.org/10.1039/c3nr34213a.

[21] J.R. Howse, R.A.L. Jones, A.J. Ryan, T. Gough, R. Vafabakhsh, R. Golestanian, Self-Motile Colloidal Particles: From Directed Propulsion to Random Walk, Phys. Rev. Lett. 99 (2007) 8–11. https://doi.org/10.1103/PhysRevLett.99.048102.

[22] S. Ketzetzi, J. de Graaf, R.P. Doherty, D.J. Kraft, Slip Length Dependent Propulsion Speed of Catalytic Colloidal Swimmers near Walls, Phys. Rev. Lett. 124 (2020) 48002. https://doi.org/10.1103/physrevlett.124.048002.

[23] R. Serra-Maia, M. Bellier, S. Chastka, K. Tranhuu, A. Subowo, J.D. Rimstidt, P.M. Usov, A.J. Morris, F.M. Michel, Mechanism and Kinetics of Hydrogen Peroxide Decomposition on Platinum Nanocatalysts, ACS Appl. Mater. Interfaces. 10 (2018) 21224–21234. https://doi.org/10.1021/acsami.8b02345.

[24] S.R.P. Pavani, M.A. Thompson, J.S. Biteen, S.J. Lord, N. Liu, R.J. Twieg, R. Piestun, W.E. Moerner, Three-dimensional, single-molecule fluorescence imaging beyond the diffraction limit by using a double-helix point spread function, Proc. Natl. Acad. Sci. U. S. A. 106 (2009) 2995–2999. https://doi.org/10.1073/pnas.0900245106.

[25] S. Ketzetzi, J. De Graaf, D.J. Kraft, Diffusion-Based Height Analysis Reveals Robust Microswimmer-Wall Separation, Phys. Rev. Lett. 125 (2020) 238001. https://doi.org/10.1103/PhysRevLett.125.238001.

[26] X. Guo, J. Wang, Comparison of linearization methods for modeling the Langmuir adsorption isotherm, J. Mol. Liq. 296 (2019) 111850. https://doi.org/10.1016/j.molliq.2019.111850.

[27] A. Nuhnen, C. Janiak, A practical guide to calculate the isosteric heat/enthalpy of adsorption: Via adsorption isotherms in metal-organic frameworks, MOFs, Dalt. Trans. 49 (2020) 10295–10307. https://doi.org/10.1039/d0dt01784a.

[28] T. Nitta, M. Kuro-Oka, T. Katayama, An adsorption isotherm of multi-site occupancy model for heterogeneous surface, J. Chem. Eng. Japan. 17 (1984) 45–52. https://doi.org/10.1252/jcej.17.45.

[29] R. Sander, Compilation of Henry's law constants (version 4.0) for water as solvent, Atmos. Chem. Phys. 15 (2015) 4399–4981. https://doi.org/10.5194/acp-15-4399-2015.

[30] S. Das, A. Garg, A.I. Campbell, J. Howse, A. Sen, D. Velegol, R. Golestanian, S.J. Ebbens, Boundaries can steer active Janus spheres, Nat. Commun. 6 (2015) 1–10. https://doi.org/10.1038/ncomms9999.

[31] C. Vericat, M.E. Vela, G. Corthey, E. Pensa, E. Cortés, M.H. Fonticelli, F. Ibañez, G.E. Benitez, P. Carro, R.C. Salvarezza, Self-assembled monolayers of thiolates on metals: A review article on sulfur-metal chemistry and surface structures, RSC Adv. 4 (2014) 27730–27754. https://doi.org/10.1039/c4ra04659e.

[32] L.O. Mark, A.H. Jenkins, H. Heinz, J.W. Medlin, Surface Science Furfuryl alcohol deoxygenation , decarbonylation , and ring-opening on Pt, Surf. Sci. 677 (2018) 333–340. https://doi.org/10.1016/j.susc.2018.07.001.

[33] P. Tereshchuk, J.L.F. Da Silva, Density functional investigation of the adsorption of ethanol-water mixture on the Pt(111) surface, J. Phys. Chem. C. 117 (2013) 16942–16952. https://doi.org/10.1021/jp403352u.

[34] E. Vesselli, G. Coslovich, G. Comelli, R. Rosei, Modelling of ethanol decomposition on Pt(111): A comparison with experiment and density functional theory, J. Phys. Condens. Matter. 17 (2005) 6139–6148. https://doi.org/10.1088/0953-8984/17/39/003.

[35] I.S. Khattab, F. Bandarkar, M.A.A. Fakhree, A. Jouyban, Density, viscosity, and surface tension of water+ethanol mixtures from 293 to 323K, Korean J. Chem. Eng. 29 (2012) 812–817. https://doi.org/10.1007/s11814-011-0239-6.

[36] S.A. Shchukarev, T.A. Tolmacheva, Solubility of oxygen in ethanol - Water mixtures, J. Struct. Chem. 9 (1968) 16–21. https://doi.org/10.1007/BF00744018.

[37] N. Singh, C.T. Campbell, A Simple Bond-Additivity Model Explains Large Decreases in Heats of Adsorption in Solvents Versus Gas Phase: A Case Study with Phenol on Pt(111) in Water, ACS Catal. (2019) 8116–8127. https://doi.org/10.1021/acscatal.9b01870.

[38] M.J. Taylor, L. Jiang, J. Reichert, A.C. Papageorgiou, S.K. Beaumont, K. Wilson, A.F. Lee, J. V. Barth, G. Kyriakou, Catalytic Hydrogenation and Hydrodeoxygenation of Furfural over Pt(111): A Model System for the Rational Design and Operation of Practical Biomass Conversion Catalysts, J. Phys. Chem. C. 121 (2017) 8490–8497. https://doi.org/10.1021/acs.jpcc.7b01744.

[39] J. Wang, C.Q. Lv, J.H. Liu, R.R. Ren, G.C. Wang, Theoretical investigation of solvent effects on the selective hydrogenation of furfural over Pt(111), Int. J. Hydrogen Energy. 46 (2021) 1592–1604. https://doi.org/10.1016/j.ijhydene.2020.10.066.

[40] H. Kahler, The crystalline structures of sputtered and evaporated metallic films, Phys. Rev. 18 (1921) 210–217.

https://doi.org/10.1103/PhysRev.18.210.

[41] M.J. Lundwall, S.M. McClure, D.W. Goodman, Probing terrace and step sites on Pt nanoparticles using Co and ethylene, J. Phys. Chem. C. 114 (2010) 7904–7912. https://doi.org/10.1021/jp9119292.

[42] A. Plauck, E.E. Stangland, J.A. Dumesic, M. Mavrikakis, Active sites and mechanisms for H2 O2 decomposition over Pd catalysts, Proc. Natl. Acad. Sci. U. S. A. 113 (2016) E1973–E1982. https://doi.org/10.1073/pnas.1602172113.

[43] S. Wang, V. Vorotnikov, D.G. Vlachos, Coverage-Induced Conformational Effects on Activity and Selectivity: Hydrogenation and Decarbonylation of Furfural on Pd(111), ACS Catal. 5 (2015) 104–112. https://doi.org/10.1021/cs5015145.

[44] S.H. Pang, J.W. Medlin, Adsorption and reaction of furfural and furfuryl alcohol on Pd(111): Unique reaction pathways for multifunctional reagents, ACS Catal. 1 (2011) 1272–1283. https://doi.org/10.1021/cs200226h.

[45] S.H. Pang, A.M. Román, J.W. Medlin, Adsorption orientation-induced selectivity control of reactions of benzyl alcohol on pd(111), J. Phys. Chem. C. 116 (2012) 13654–13660. https://doi.org/10.1021/jp303147c.

[x] Zare, M.; Saleheen, M. S.; Singh, N.; Uline, M. J.; Faheem, M.; Heyden, A. Liquid Phase Effects on Adsorption Processes in Heterogeneous Catalysis. Submitt. to Nat. Commun. 2021.